

# A Simple Targeting Procedure for Lunar Trans-Earth Injection

Shane B. Robinson\* and David K. Geller†

*Utah State University, Logan, Utah, 84322, USA*

A simple targeting algorithm for lunar trans-Earth injection is developed. This algorithm builds on techniques developed for the Apollo program and other lunar and interplanetary missions. The simplicity and robustness of this particular algorithm makes it well-suited for onboard use during contingency and abort operations. Rather than attempting to create fuel-optimal trajectories, the algorithm presented in this paper focuses on computing a trajectory from low lunar orbit to direct atmospheric Earth entry that minimized the time of flight but does not violate the fuel constraint. The number of impulses executed is also minimized. This algorithm has three stages. First, an estimate of the hyperbolic excess velocity at the Lunar sphere of influence is generated. Second, a maneuver is computed using conic techniques that will transfer the craft from a lunar circular orbit to the hyperbolic escape asymptote. Finally, the effects of perturbations are eliminated by using fixed-time linear targeting methods. Some examples demonstrating the effectiveness of the targeting algorithm are also presented. The algorithm can also be used to quickly generate good initial guesses for other trajectory optimization algorithms.

## I. Introduction

The goal of this paper is to present the theory and development for a simple and robust targeting algorithm intended for onboard use during contingency and abort scenarios where a spacecraft needs to return to the Earth from an arbitrary circular lunar orbit. There are several historically significant papers,<sup>1-3</sup> which detail the optimization of the transfer from a low parking orbit to a hyperbolic escape asymptote. However, the theories presented in the literature are built around Keplerian motion and do not account for the highly perturbed nature of the gravity field in cislunar space. This research is aimed at producing an algorithm based on existing injection theory coupled with other targeting techniques to solve the trans-earth injection (TEI) problem. Since the Apollo program some advancements have been made. However, these more recent techniques are more complex and generally require a good initial guess in order to guarantee convergence. In many instances generating these initial guess can be a painstaking process that requires substantial human input. This makes these methods potentially ill suited for onboard applications particularly during emergency situations when CPU resources may be limited, ground communications cut, or when unforeseen initial conditions may exist.

Although only a single impulse was used for trans-Earth injection during the Apollo mission, NASA's current proposed lunar mission is much more technologically demanding than the Apollo lunar missions. The Apollo lunar trajectories, and missions in general, were heavily constrained for a variety of reasons, most of these relating to the limitations of the Apollo spacecraft, and the constraints on ground support available. The new mission demands that technologies be developed that will allow many of these constraints to be relaxed, or removed completely. These new requirements demand that the new spacecraft have a much greater ability to execute autonomous operations. For example, the Apollo craft had a very narrow, predetermined window for return, and relied on ground support to upload the guidance solution for TEI. Current requirements for lunar missions dictate that the spacecraft must be able to return from the Moon

\*Graduate Student, Mechanical and Aerospace Engineering, 4130 Old Main Hill, AIAA Student Member.

†Assistant Professor, Mechanical and Aerospace Engineering, 4130 Old Main Hill, AIAA Senior Member.

to Earth at any time and from any lunar orbit. In the event that communications with the Earth are interrupted, the spacecraft must be able to execute TEI completely autonomously. New techniques that are focused on autonomous operations need to be developed for nearly all phases of lunar flight. The methods proposed in this paper, are intended to calculate the TEI sequence onboard the spacecraft.

Although the methods in this paper are targeted at performing an autonomous TEI maneuver, they may also be used to replace the human that is often heavily involved in producing initial trajectories for optimization routines that rely on linearization. With minor modifications, the approach in this paper can be used to compute a multi-impulse lunar orbit insertion (LOI) maneuver.

The limited computing power available onboard the craft and the limited time available for performing the computations, demand that procedures for calculating the TEI sequence must be simple yet robust. The algorithm in this paper attempts to accomplish this simplicity and robustness by using the amount of available propellant as a constraint while minimizing the time-of-flight rather than trying to use the minimal amount of fuel.

As the angle between the plane of the lunar orbit and the hyperbolic escape asymptote becomes large, the limited fuel available requires the maneuver to consist of multiple impulses.<sup>1</sup> Although only a single impulse was used for the trans-earth injection during the Apollo mission, double and triple impulse TEI procedures were studied during the Apollo mission design process.<sup>4-7</sup> These studies clearly showed the advantages of multi-impulse maneuvers in providing global access to the moon. The principal advantages of these multi-impulse trajectories was their ability to provide access to more of the lunar surface and substantially increase the payload that could be returned from the moon. However, these multi-impulse procedures added substantial complexity to mission design and execution and were ultimately not used during Apollo.

In this paper these techniques will be revisited and integrated into a new simple and robust targeting algorithm. This algorithm is intended for onboard use during contingency and abort scenarios where a spacecraft needs to return to the Earth from an arbitrary circular lunar orbit. These techniques may also be useful in generating initial guesses for trajectories during mission planning.

### **I.A. The Need to Minimize Fuel Use**

During the mission planning phase it is desirable to find fuel-optimal trajectories. The cost of carrying the additional mass associated with unneeded fuel on the spacecraft is so large that every possible reduction in fuel results in substantial savings. Once a mission launches, mission assurance replaces issues such as fuel savings as the primary metric for decision making. Mission assurance is weighted even heavier should a mission enter contingency and abort operations. This algorithm was constructed for the latter mission model. Nevertheless, it may still have utility during the former as a technique for reliably and rapidly producing good initial guess for other more sophisticated iterative optimization algorithms which do attempt to minimize the fuel usage.<sup>8,9</sup>

In abort and contingency operations there is little use in minimizing the fuel usage. Any fuel not used to execute maneuvers will be discarded or returned to Earth unused. After launch the cost to the mission is fixed, regardless of the amount of fuel used to execute the required maneuvers. Therefore, in abort and contingency operations it is desirable to consider fuel available as a constraint rather than a parameter that should be optimized. In these situations, rather than minimizing the fuel consumed by the maneuver, it may be more appropriate to minimize parameters that could pose a more immediate danger to the mission, such as the return time,<sup>10</sup> the number and the complexity of impulses required to execute the maneuver, or in some cases atmospheric interface velocity.

Each impulse causes an increase in the complexity and thus the risk of failure for the mission. Furthermore, each successive impulse adds substantially to the total time of return. These two effects are generally undesirable for manned missions and are particularly unfavorable for abort situations. This algorithm attempts to avoid excessive impulses and keep the time required to return to the Earth to a minimum. The algorithm also attempts to keep these factors at a minimum by simply trying to use as few impulses as possible. In order to accomplish this, the one- and two- impulse methods seek to minimize fuel use, while the three impulse maneuver attempts to minimize the time spent in intermediate transfer orbits by consuming all of the available fuel. In all these cases, the primary goal is to limit the number of impulsive maneuvers, with the secondary goal of minimizing the time of flight.

## I.B. Algorithm Overview

The algorithm can be summarized as follows

1. An estimate of the  $\vec{V}_\infty$  is generated. This is accomplished by applying boundary constraints appropriate for atmospheric entry to Lambert's time-of-flight equation. The effects of non-Keplerian gravity are then removed with an iterative procedure, and an estimate of the velocity at the lunar SoI is determined. The minimum time-of-flight is chosen to correspond to the maximum allowable atmospheric entry velocity.
2. The injection sequence that transfers the spacecraft from a circular lunar orbit to  $\vec{V}_\infty$  is computed. This is accomplished by choosing the minimum number of impulses subject to a fuel constraint. For the triple-impulse procedure the time required to traverse the transfer ellipses is also minimized.
3. Linear state transition matrix targeting is used to enforce the desired boundary constraints at atmospheric interface in a non-Keplerian gravitational environment.

## II. Generating $\vec{V}_\infty$

The first step involves finding the velocity at the moon's SoI,  $\vec{V}_{SoI}$ , at a desired epoch that will produce a lunar return trajectory which meets the desired entry conditions at the Earth. This vector defines the escape asymptote,  $\hat{i}_{\vec{V}_{SoI}}$ , and the velocity at the SoI,  $V_{SoI}$ . The velocity at the SoI can be used to generate a good approximation of the hyperbolic excess velocity,  $\vec{V}_\infty$ .  $\vec{V}_{SoI}$  is very nearly identical to  $\vec{V}_\infty$  in direction but differs more significantly in magnitude. The vis-viva equation can be used to relate  $V_\infty$  and  $V_{SoI}$  in terms of,  $r_{SoI}$ , the radius of the sphere of influence, and  $\mu_m$ , the gravitational parameter of the moon.

$$V_\infty^2 = V_{SoI}^2 - 2 \frac{\mu_m}{r_{SoI}} \quad (1)$$

This can be used to generate a good approximation

$$\vec{V}_\infty \approx V_\infty \frac{\vec{V}_{SoI}}{V_{SoI}} \quad (2)$$

In order to be useful onboard a spacecraft, a method for finding  $\vec{V}_{SoI}$  must be capable of running reliably with the computational assets available onboard the spacecraft. Any method used onboard the spacecraft must also be robust, and always converge to the correct solution. One possible method for generating  $\vec{V}_\infty$  for elliptic return trajectories of any epoch is outlined in this section. However, it should be noted that the technique for generating  $\vec{V}_\infty$  outlined here can be replaced without effecting the second and third stages outlined in this paper for computing the TEI sequence. The second and third stages will work regardless of the method used to produce  $\vec{V}_\infty$ .

The computational speed of the method for finding  $\vec{V}_\infty$  proposed here is almost entirely dependent on the speed of the trajectory integrator used. In fact, compared to performing the integration the computational time required for the other portions of the method is negligible. Thus, given a sufficiently rapid trajectory integration technique this method could conceivably be placed onboard the spacecraft. In the absence of a rapid integration scheme, tables of  $\vec{V}_\infty$  can be computed a priori and stored onboard. Using table lookups it is possible to find  $\vec{V}_\infty$  rapidly regardless of the method used to compute it. Computing these values before flight allows for more sophisticated boundary constraints than the techniques outlined here allow. Thus, the method presented here might be replaced with a some other method that generates tables of  $\vec{V}_{SoI}$  which are then stored onboard the spacecraft. However, this method is attractive because of its relative simplicity and robustness.

The method for computing  $\vec{V}_\infty$  presented here is loosely based on a method outlined by Battin<sup>11</sup> for obtaining the two-body solution. The notation used by Battin will be followed here as closely as possible. The approach outlined by Battin is extended by replacing the boundary conditions on the terminal end of the trajectory with conditions more appropriate for a direct atmospheric entry. An iterative technique that corrects for the effects of perturbations on the trajectory is also presented.

The boundary conditions used are:

- A target vector,  $\vec{r}_T$ . This is a vector from the center of mass of the Earth to a point on the lunar SoI. This vector represents the point where the spacecraft emerges from the SoI. Thus, this vector is associated with,  $t_{SoI}$ , the epoch when the spacecraft pierces the SoI.
- The inclination of the return orbit with respect to the Earth's equatorial plane,  $i_R$ . Retrograde returns have the undesirable effect of raising the velocity relative to the atmosphere unnecessarily. Posigrade returns have the opposite effect. For this reason retrograde returns will not be considered. Since only posigrade orbits are considered,  $i_R$  exists on the interval  $|\delta_T| \leq i_R \leq \frac{\pi}{2}$ , where  $\delta_T$  is the declination of  $\vec{r}_T$ .
- The flight path angle at entry interface,  $\gamma_i$ . For atmospheric entry this will always be a negative value.
- The radial distance at entry interface,  $r_i$ . This value is assumed to be constant with respect to entry latitude. The  $\sim 20$  km difference in earth radius between the pole and the equator and other variations in the interface altitude are neglected.
- Either a north-to-south entry or a south-to-north entry must be selected. If  $i_R \geq \delta_T$  then there are two orbital planes of inclination  $i_R$  which contain the target vector  $\vec{r}_T$ . This selection resolves the ambiguity between these two planes.
- The desired time-of-flight from the SoI to atmospheric interface,  $t_{FR}$ . This value is constrained by the requirement that the return trajectory must be elliptic. The constraints on this value will be discussed in section II.A.1.

## II.A. The Conic Boundary Value Problem

The geometry of these constraints is shown in figure 1. Note that the absolute value of the flight path angle is shown in the figure and will be used occasionally in the equations. When the absolute value is used it will always be indicated with  $|\cdot|$ .

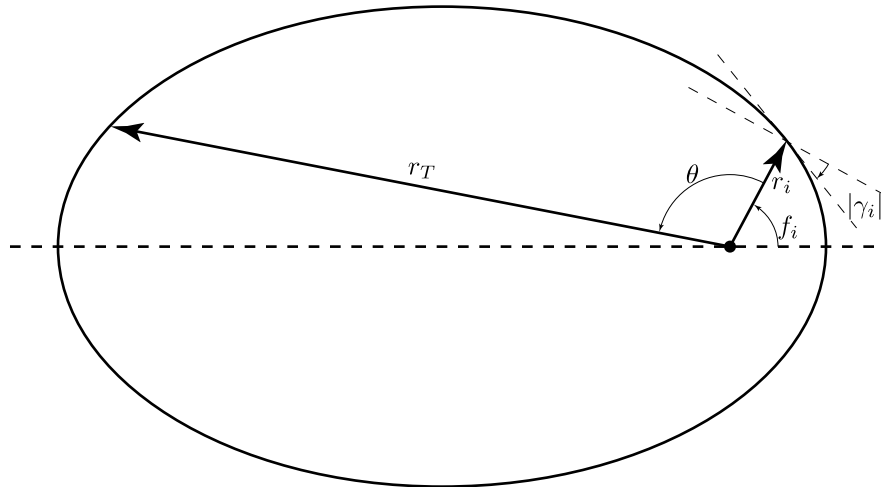


Figure 1. The geometry of these constraints for an ellipse.

If  $f_i + \theta > \pi$  the spacecraft will be moving away from the Earth when it exits the SoI. Such a trajectory serves only to increase the time-of-flight. Therefore these trajectories are disregarded and it is assumed that  $f_i + \theta < \pi$ . The conic orbit allows three equations describing the geometric constraints to be written.

$$r_i = \frac{p}{1 + e \cos(f_i)} \quad (3)$$

$$r_T = \frac{p}{1 + e \cos(f_i + \theta)} \quad (4)$$

$$\tan |\gamma_i| = \frac{e \sin(f_i)}{1 + e \cos(f_i)} \quad (5)$$

where  $p$  is the parameter of the orbit, and  $e$  is the eccentricity of the orbit.

These equations can be rearranged to express  $p$ ,  $e$ , and  $f_i$  as functions of the central angle  $\theta$ . First the nondimensional value  $B$  is introduced

$$B = e \cos(f_i) = \frac{r_T [1 - \tan |\gamma_i| \sin(\theta)] - r_i}{r_i - r_T [\cos(\theta) - \tan |\gamma_i| \sin(\theta)]} \quad (6)$$

together with

$$e \sin(f_i) = \tan |\gamma_i| (1 + B) \quad (7)$$

Equation 6 clearly indicates that  $f_i = \frac{\pi}{2}$  when  $B = 0$ . Also note that  $|B| < 1$  for elliptic orbits. The quotient of equations 6 and 7 can be used to temporarily remove  $e$  from the problem and find an expression for  $f_i$

$$\tan(f_i) = \tan |\gamma_i| \frac{1 + B}{B} \quad (8)$$

The true anomaly at atmospheric interface,  $f_i$ , can now be used to find the eccentricity

$$e = \begin{cases} \frac{B}{\cos(f_i)} & B \neq 0 \\ \tan |\gamma_i| & B = 0 \end{cases} \quad (9)$$

At this point the value of  $e$  should be checked to insure that  $\theta$  corresponds to an elliptic trajectory. If the trajectory is elliptic, the parameter and semi-major axis of the ellipse,  $a$ , can now be found

$$p = r_i (1 + B) \quad (10)$$

and

$$a = \frac{p}{1 - e^2} \quad (11)$$

With these values Lambert's time-of-flight equation for elliptic orbits can be used to find the time-of-flight as a function of  $\theta$ .

$$t_{FR} = \sqrt{\frac{a^3}{\mu_e}} [\alpha_1 - \sin(\alpha_1) - \alpha_2 + \sin(\alpha_2)] \quad (12)$$

where  $\mu_e$  is the gravitational parameter for the Earth. The angles  $\alpha_1$  and  $\alpha_2$  are given by

$$\sin\left(\frac{\alpha_1}{2}\right) = \sqrt{\frac{s}{2a}} \quad (13)$$

$$\sin\left(\frac{\alpha_2}{2}\right) = \sqrt{\frac{s-c}{2a}} \quad (14)$$

Note that because of the restriction  $\theta + f_i < \pi$ , the quadrant ambiguity for  $\alpha_1$  and  $\alpha_2$  is avoided. The semi-perimeter,  $s$ , and cord length,  $c$ , are given by

$$c^2 = r_i^2 + r_T^2 - 2r_i r_T \cos(\theta) \quad (15)$$

and

$$2s = r_i + r_T + c \quad (16)$$

The  $t_{FL}$  is now expressed entirely as a function of  $\theta$ .

A simple Newton-Raphson technique can be used to quickly find  $\theta$  given  $t_{FL}$ . This requires finding the derivative of  $t_{FL}$  with respect to  $\theta$ .

$$\frac{dt_{FR}}{d\theta} = \frac{3}{2} t_{FR} \left( \frac{1}{a} \frac{da}{d\theta} \right) + \sqrt{\frac{a}{\mu_e}} \left[ \tan\left(\frac{\alpha}{2}\right) \left( \frac{ds}{d\theta} - s \frac{1}{a} \frac{da}{d\theta} \right) + \tan\left(\frac{\beta}{2}\right) \left( \frac{ds}{d\theta} + (s-c) \frac{1}{a} \frac{da}{d\theta} \right) \right] \quad (17)$$

The derivative of the semi-perimeter is

$$\frac{ds}{d\theta} = \frac{r_i r_T}{2a} \sin(\theta) \quad (18)$$

The chain rule can be used to find the other needed derivative

$$\frac{1}{a} \frac{da}{d\theta} = \frac{1}{a} \frac{da}{dB} \frac{dB}{d\theta} \quad (19)$$

where

$$\frac{1}{a} \frac{da}{dB} = \begin{cases} \frac{1}{1+B} + \frac{2}{B} \frac{1 - \frac{\tan|\gamma_i| \sin(f_i)}{e^{-2}-1}}{e^{-2}-1} & B \neq 0 \\ \frac{1}{2 \cos^2(\gamma_i) - 1} & B = 0 \end{cases} \quad (20)$$

This equation is only singular for elliptic orbits when both  $f_e = \frac{\pi}{2}$  ( $B = 0$ ) and  $|\gamma_i| = \frac{\pi}{4}$  are true. These conditions correspond to a class of trajectories that are of little interest for lunar return. Finally, the last derivative required is given by

$$\frac{dB}{d\theta} = \frac{B [\sin(\theta) + \tan|\gamma_i| \cos(\theta)] + \tan|\gamma_i| \cos(\theta)}{\cos(\theta) - \tan|\gamma_i| \sin(\theta) - \frac{r_i}{r_T}} \quad (21)$$

Note that equation 21 has a singularity at exactly the same points as equation 6<sup>a</sup>. It can be shown that when  $r_i < r_T$  these equations can only be singular when  $\theta \leq \frac{\pi}{2} - |\gamma_i|$ . For the lunar return problem ( $\frac{r_i}{r_T} \approx 0.01$ ) values of  $\theta$  which satisfy this constraint correspond to hyperbolic trajectories. In addition to being hyperbolic, trajectories that produce singularities in equation 21 have undesirably large values for  $|\gamma_i|$ .

For the lunar return problem experience has shown 2.8 rad ( $\sim 160^\circ$ ) is a good initial guess for starting the Newton-Raphson solver.

### II.A.1. Time-of-Flight Constraints

Bate and colleagues<sup>12</sup> find an approximate value for the upper bound on  $t_{FL}$  by disregarding the gravity of the moon and considering an elliptic orbit with a major axis equal to the average Earth-moon distance. Half the period of an orbit with a semimajor axis of 385,000 km is nearly 5 days ( $\sim 120$  hr). Thus a spacecraft traveling between the moon and the Earth on a conic trajectory with a time-of-flight larger than 5 days must reach an apogee farther from the Earth than the moon. The long time-of-flight for these trajectories make them unsuitable for lunar return.

When trajectories are computed using the technique in this paper  $t_{FR}$  does not include the portion of the trajectory inside the lunar sphere of influence. From the sphere of influence the maximum time-of-flight has been found empirically to be  $\sim 3.5$  days when the moon is near it's closest approach to Earth and  $\sim 4.0$  days when the moon is at its farthest distance from Earth. Since the quickest return to earth possible is desirable for several reasons<sup>10</sup> this upper limit on flight time should never be encountered for the lunar return problem. This does become a constraint for the trip to the moon when minimizing the orbital energy is more desirable, as in the case of LOI.

The parabolic time-of-flight,  $t_{FR(p)}$ , is used to as a lower limit on  $t_{FR}$ . Barkers equation can be used to derive a expression for the parabolic time-of-flight between two radial distances<sup>b</sup> ( $r_T < r_i$ ).

$$t_{FL(p)} = \frac{1}{3\sqrt{\mu_e}} \left[ \sqrt{2r_T - p} (r_T + p) - \sqrt{2r_i - p} (r_i + p) \right] \quad (22)$$

For highly eccentric orbits with shallow flight path angle at atmospheric interface, like lunar return orbits, the parabolic time-of-flight may be well approximated without the parameter  $p$

$$t_{FR(p)} \approx \frac{1}{3} \sqrt{\frac{2(r_T - r_i)}{\mu_e}} (r_T + 2r_i) \quad (23)$$

<sup>a</sup>This equation is singular when  $\frac{r_i}{r_T} \cos(|\gamma_i|) = \cos(\theta + |\gamma_i|)$ . When  $\frac{r_i}{r_T} \ll 1$  the location of this singularity is well approximated by  $\frac{\pi}{2} = \theta + |\gamma_i|$ .

<sup>b</sup>The equation assumes that the trajectory does not reach periape between the end points defined by  $r_T$  and  $r_i$ . If periape were to occur between these two points then the two terms in this equation must be added rather than differenced.

which describes the parabolic time-of-flight between a radial distance,  $r_T$  to an periaipse radius of  $r_i$ . For lunar return trajectories the value of  $t_{FR(p)}$  has been found empirically to be  $\sim 1.7$  days when the moon is near it's closest approach to Earth and  $\sim 2.1$  days when the moon is at its farthest distance from Earth.

## II.B. Finding the Position and Velocity Vectors at the Boundaries

The inclination constraint,  $i_R$ , together with the declination,  $\delta_T$ , and the right ascension,  $\lambda_T$ , of the target vector can be used to find the orbit normal vector. The right ascension of the ascending node for the return orbit with an atmospheric entry from the north to the south is given by

$$\Omega_N = \lambda_T - \sigma \quad (24)$$

Similarly, the right ascension of the ascending node for an entry from the south to the north is given by

$$\Omega_S = \lambda_T + \sigma + \pi \quad (25)$$

where the the angle  $\sigma$  is given by the spherical trigonometric relationship

$$\sin(\sigma) = \frac{\tan(\delta_T)}{\tan(i_R)} \quad (26)$$

The unit vector normal to the return orbit is given by

$$\hat{i}_{\vec{h}_i} = \begin{bmatrix} \sin(\Omega) \sin(i_R) \\ -\cos(\Omega) \sin(i_R) \\ \cos(i_R) \end{bmatrix} \quad (27)$$

It is now a simple procedure to find the state vectors at each end of the conic arc. The position vector at atmospheric interface is a linear combination of known unit vectors.

$$\vec{r}_i = r_i \left[ \cos(\theta) \hat{i}_{\vec{r}_T} + \sin(\theta) \left( \hat{i}_{\vec{h}} \times \hat{i}_{\vec{r}_T} \right) \right] \quad (28)$$

With the position vectors for both ends of the trajectory, their accompanying velocity vectors may now be found by considering the radial and tangential components of the velocity separately.

$$\vec{v}_i = -e \sqrt{\frac{\mu_e}{p}} \sin(f_i) \hat{i}_{\vec{r}_i} + \frac{\sqrt{\mu_e p}}{r_i} \left( \hat{i}_{\vec{h}} \times \hat{i}_{\vec{r}_i} \right) \quad (29)$$

$$\vec{v}_i = -e \sqrt{\frac{\mu_e}{p}} \sin(f_i + \theta) \hat{i}_{\vec{r}_T} + \frac{\sqrt{\mu_e p}}{r_T} \left( \hat{i}_{\vec{h}} \times \hat{i}_{\vec{r}_T} \right) \quad (30)$$

## II.C. Iterative Procedure

Due the highly non-Keplerian nature of cislunar space, an iterative procedure must be used to remove the effects of perturbations. This section contains an iterative procedure for removing the resulting trajectory defects. As was mentioned previously, the time required for a computer to compute this solution is almost entirely dependent on the time required to numerically integrate the trajectory. This procedure attempts to minimize the number of trajectory integrations required for convergence.

The iterative procedure consists of two phases:

1. Using the equations for conic arcs which from the preceding section, the target vector,  $\vec{r}_T$ , is moved across the sphere of influence with the objective of aligning the moon relative position and velocity vectors. Aligning these vectors is equivalent to an aiming radius,  $r_a$ , of zero. The result of this phase is an initial estimate of  $\vec{r}_T$  which does not include the effects of perturbations.
2. An iterative procedure is used to update  $\vec{v}_T$  to include the effects of perturbations on the trajectory. The target vector,  $\vec{r}_T$ , is once again moved on the SoI to force the aiming radius to vanish. Each time the target vector is moved  $\vec{v}_T$  is updated to include the effects of perturbations.

This procedure requires an initial guess. A good first guess for the lunar return problem has been found empirically. This guess is a function of,  $\vec{r}_M$ , the position and  $\vec{v}_M$ , the velocity of the moon with respect to the Earth.

$$(\vec{r}_{TM})_0 = -r_{SoI} \left( \frac{1}{2} \frac{\vec{r}_M}{r_M} + \frac{\sqrt{3}}{2} \frac{(\vec{v}_M \times \vec{r}_M) \times \vec{r}}{|\vec{v}_M \times \vec{r}_M|} \right) \quad (31)$$

The geometric interpretation of this relation can be seen by remembering  $\cos(\frac{\pi}{6}) = \frac{\sqrt{3}}{2}$ , and  $\sin(\frac{\pi}{6}) = \frac{1}{2}$ .

The first step of the iterative procedure involves driving the  $r_a$  produced by conic trajectories from the earth to the lunar SoI to zero by iterative placement of  $\vec{r}_T$  on the SoI.

The aiming radius is found by first finding the unit vector that points at the aiming point.

$$\hat{i}_a = \frac{\vec{v}_{TM} \times (\vec{r}_{TM} \times \vec{v}_{TM})}{|\vec{v}_{TM} \times (\vec{r}_{TM} \times \vec{v}_{TM})|} \quad (32)$$

The  $M$  appended to the subscript indicates vectors with respect to the moon rather than the Earth. The vector from the moon to the aiming point is now simply the projection of the  $\vec{r}_{TM}$  onto  $\hat{i}_a$ .

$$\vec{r}_a = (\vec{r}_{TM} \cdot \hat{i}_a) \hat{i}_a \quad (33)$$

When  $r_a$  is greater than 32000 km the target vector can be corrected by subtracting  $\vec{r}_a$  from the moon relative target vector  $\vec{r}_{TM}^-$ . The new target is then placed on the SoI by adjusting it's magnitude.

$$\vec{r}_{TM}^+ = r_{SoI} \frac{\vec{r}_{TM}^- - \vec{r}_a}{|\vec{r}_{TM}^- - \vec{r}_a|} \quad (34)$$

When  $r_a$  is less than 32000 km Battin suggests an approach for updating  $\vec{r}_T$  by taking advantage of the fact that moving the target vector a small amount does not cause large alterations to the velocity at the target.<sup>c</sup>

$$\vec{r}_{TM}^+ = r_{SoI} \frac{\vec{v}_{TM}^-}{v_{TM}^-} \quad (35)$$

The trajectory can be corrected to compensate for the effects of perturbations once a target vector that produces an aiming radius of less than a tolerance  $\varepsilon_a$  (1 km works well) has been found. The effects of perturbations are removed by integrating the trajectory backwards from the interface conditions generated by the conic solution to the time when the conic solution pierces the SoI. Based on the difference between  $\vec{r}_T$  and the final state delivered by the integrator,  $\vec{r}_d$ , corrections are applied. This integration routine can contain any force models for which the trajectory need correction. However, at this point a precision solution is not necessary. Only perturbations which have a large effect on the trajectory should be considered. The effects of smaller perturbations can be removed at a later stage by using more precise models during the differential correction stage.

The error between the position delivered by the integrator,  $\vec{r}_d$ , and the target is found

$$\vec{\varepsilon}_k = \vec{r}_T - (\vec{r}_d)_k \quad (36)$$

This error vector can now be used to bias the target vector

$$(\vec{r}'_T)_k = (\vec{r}'_T)_{k-1} + \vec{\varepsilon}_k \quad (37)$$

with the initial condition

$$(\vec{r}'_T)_0 = \vec{r}_T \quad (38)$$

The biased target vector,  $(\vec{r}'_T)_k$ , is then used to compute a conic arc. This procedure is repeated until the error vector drops below some acceptable value,  $\varepsilon_\varepsilon$ . The first portion of this iterative process is described graphically in figure 2. This procedure is similar to the so called modified Lambert targeting used to correct

<sup>c</sup>In the limit both of these update strategies are equivalent.

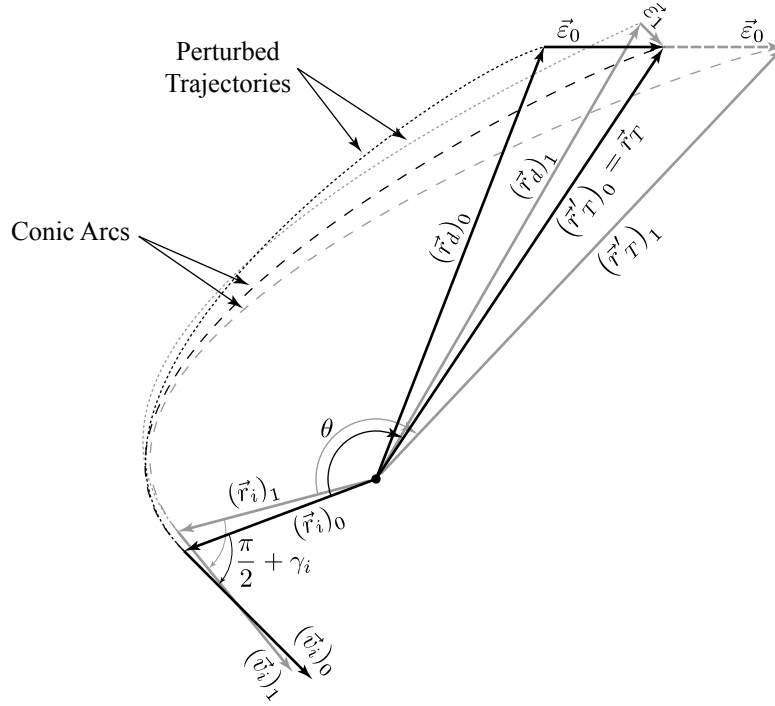


Figure 2. One iteration of the iterative targeting procedure.

for J2 perturbations. The main difference is that  $\vec{r}_i$  is not fixed but moves with each iteration to accommodate the boundary conditions.

Once the trajectory has been corrected for perturbations the aiming radius is no longer zero. The target vector is then moved using the technique in equation 35. This process is then repeated until the aiming radius vanishes. Each time  $\vec{r}_T$  is moved the effects of perturbations must be removed again. Substantial computational effort can be avoided during this process by simply changing  $\vec{r}'_T$  to reflect the change in  $\vec{r}_T$  rather than equating the two after a new estimate for  $\vec{r}_T$  is found.

$$(\vec{r}'_T)_k = (\vec{r}'_T)_{k-1} + (\vec{r}_T^+ - \vec{r}_T^-) \quad (39)$$

Once a final value for  $\vec{V}_{SoI}$  is found the corrections in equations 1 and 2 need to be applied to obtain  $\vec{V}_\infty$ . Figure 3 contains a flow chart describing the entire process.

#### II.D. Minimizing $t_{FR}$

Numerous strategies could be used for selecting  $t_{FR}$  to meet a variety of mission objectives. One particularly attractive scheme, especially in abort or contingency operations, is to minimize  $t_{FR}$ . Minimizing  $t_{FR}$  has a desirable effect on mission success, by helping to minimize the probability of failure.<sup>10</sup> One of the consequences of the Lambert time-of-flight equation (equation 12) is that the partial derivative of orbital energy with respect to time of flight is always negative. This is convenient because atmospheric interface velocity can be viewed as measure of orbital energy if the inclination is held constant. It can then be reasonably assumed that the minimum time-of-flight associated with the given boundary conditions is the time-of-flight associated with the maximum allowed atmospheric entry velocity.

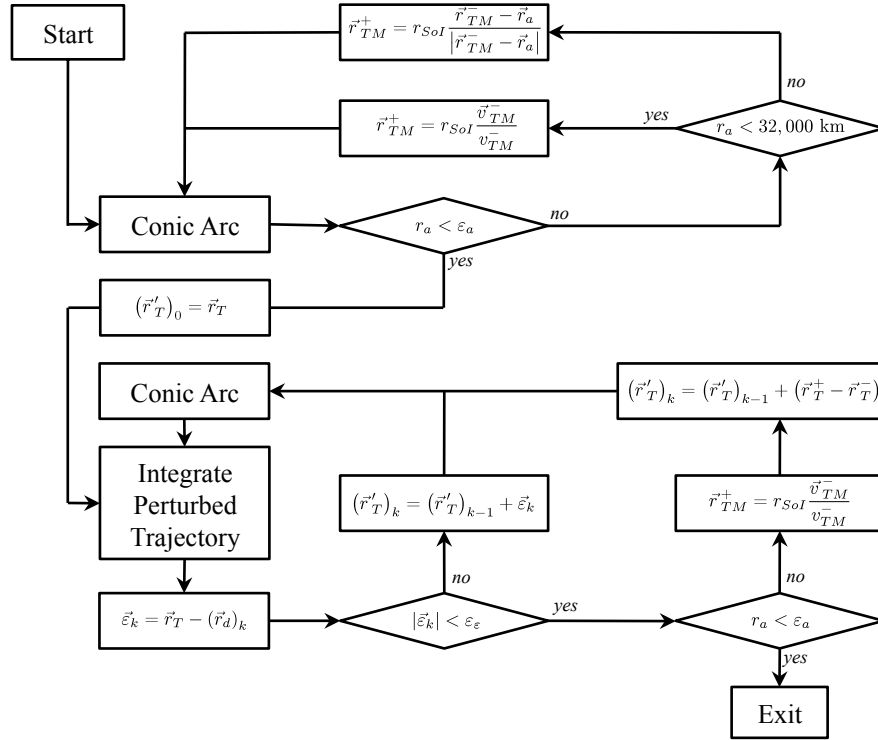


Figure 3. Flow Chart.

### III. Multi-Impulse Injection

This section outlines the method used for computing the impulsive maneuver, or sequence of impulsive maneuvers, needed to transfer the spacecraft from a circular lunar orbit to a desired hyperbolic escape asymptote.

This method attempts to minimize the number of maneuvers needed for lunar return, without exceeding the fuel available for the maneuver. This operational approach strives to make use of all  $\Delta V$  capacity available for the maneuver, rather than seeking to produce a truly fuel-optimal trajectory. In other words, this method does not increase the number of impulses in order to use less fuel. Rather, this method seeks to perform the minimal number of impulses, without exceeding the  $\Delta V$  capacity available to execute the maneuver.

Selecting the correct number of maneuvers needed to execute the injection sequence consists of simply selecting the simplest maneuver that does not violate the  $\Delta V$  constraint. If the one and two maneuver sequences violate the constraint, then the three maneuver sequence that minimizes the period of the transfer orbits by consuming all of the  $\Delta V$  available for the maneuver is computed.

#### III.A. Single-Impulse Maneuver

The simplest TEI maneuver is a single-impulse maneuver like the trajectory shown in Figure 4. The Apollo missions were carefully designed in order to use only a single impulse to return. The single-impulse maneuver is only possible when the hyperbolic escape asymptote is located in or very near the orbital plane of the lunar parking orbit. Keeping the escape asymptote in or near the orbital plane has the effect of allowing the vast majority of the fuel to be used for boosting the orbital energy of the craft rather than performing a plane change.

Gunther<sup>3</sup> develops a method for computing the fuel-optimal single impulse maneuver that will execute a transfer from a circular orbit to a hyperbolic escape asymptote. The details of Gunther's development are omitted here, but the equations required to perform the needed calculations will be presented. The notation

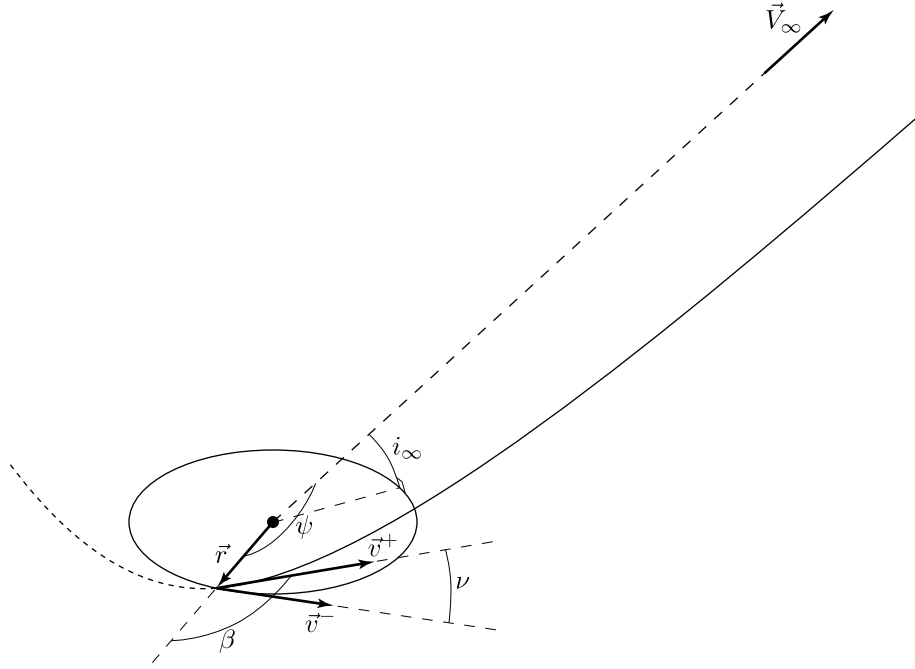


Figure 4. The geometry of the single-impulse trans-earth injection maneuver. The impulse is executed at perigee of the hyperbolic escape trajectory. This impulse consists of a minimal plane change and a large energy boost. This single impulse places the craft on a trajectory that will intercept the Earth's atmosphere for direct entry.

is consistent with Gunther whenever possible.

At the core of Gunther's single impulse method is a fourth degree polynomial in  $w$ . The parameter  $w$  has no apparent geometric meaning, and is used only as a convenient medium for producing a tractable solution.

$$w^4 - Kw^3 - K \sin^2(i_\infty)w - \sin^2(i_\infty) = 0 \quad (40)$$

The parameter  $K$  is the the nondimensional hyperbolic escape velocity.

$$K = \frac{V_\infty}{V_{circ}} \quad (41)$$

For a circular lunar orbit with a period of  $\sim 2$  hr, and time-of-flight constraints discussed in section II.A.1, bounds can be placed on the values of  $K$  for the lunar return originating at a 100 km orbit. In this situation  $0.5 \lesssim K \lesssim 0.9$ . Nevertheless, these equations are valid for any  $K > 0$ .

Descarte's rule guarantees that equation 40 has one positive real root, which is associated with the single impulse fuel optimal maneuver. The positive real root corresponds to an injection after periapse of the hyperbolic trajectory. This has the added advantage of never impacting the moon.

The parameter  $w$  can then be used to calculate,  $\beta$ , the compliment of the flight path angle immediately after the impulse.

$$\cos(\beta) = \frac{w - K}{\sqrt{K^2 + 2}} \quad (42)$$

The eccentricity of the hyperbolic trajectory is given by the relation

$$e^2 = (K^2 + 1)^2 - K^2(K^2 + 2)\cos^2(\beta) \quad (43)$$

With the eccentricity, the angle between position vector at the location of the impulse and the escape asymptote can be computed

$$\psi = \cos^{-1}\left(\frac{-1}{e}\right) - \cos^{-1}\left[\frac{1}{e}\left(\frac{e^2 - 1}{K^2} - 1\right)\right] \quad (44)$$

The angle  $\nu$ , is the angle between the velocity vector immediately prior to the impulse and the velocity vector immediately after the impulse.

$$\cos(\nu) = \sin(\beta) \sqrt{1 - \frac{\sin^2(i_\infty)}{\sin^2(\psi)}} \quad (45)$$

Given these values the position and velocity vectors that define the impulse can readily be computed. The required magnitude of the maneuver can also be computed directly

$$\frac{\Delta V_1}{V_{circ}} = \sqrt{K^2 + 3 - 2\sqrt{(1 + Kw - w^2)(2 + Kw)}} \quad (46)$$

Figure 5 contains a plot showing the  $\Delta V$  cost for the one impulse maneuver.

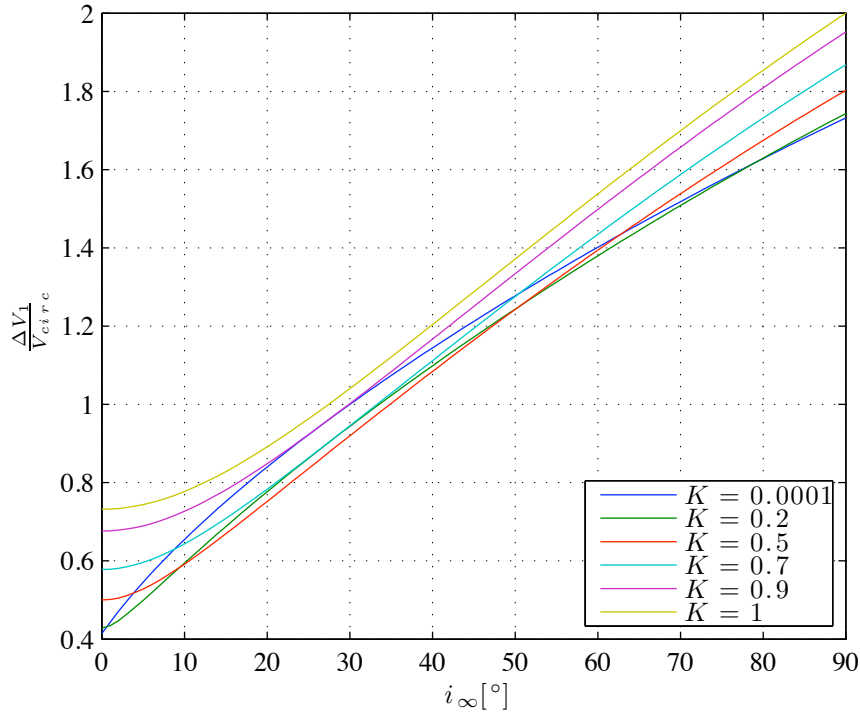


Figure 5. Nondimensional impulse magnitude as a function of  $K$  and  $i_\infty$ .

### III.B. Double-Impulse Maneuver

For larger values of  $i_\infty$ , the limited fuel available requires that the maneuver consist of multiple impulses. As  $i_\infty$  increases, the fuel needed to execute the plane change portion of the maneuver using a single-impulse increases dramatically, as can be seen in figure 5. This dramatic increase in the fuel required is avoided by using multiple impulses to execute the maneuver rather than just one impulse.

The geometry of the two-impulse maneuver is shown in Figure 6. The first impulse is similar to the single-impulse maneuver. It does include a minimal plane change, but the primary purpose of the first impulse is to boost the orbital energy of the spacecraft. This impulse places the spacecraft on an intermediate low-energy hyperbolic escape trajectory. The second impulse is performed at or near the sphere of influence. This is a large impulse that executes the remainder of the plane change and places the spacecraft on the desired departure asymptote.

Gunther is able to compute an optimal solution to this maneuver by assuming that the second impulse is executed at an infinite distance from the central body. In this paper the infinite distance is approximated



If the value for  $i_1$  is greater than  $i_\infty$  then the two impulse procedure is not necessary and the single impulse solution should be used. At this point  $K_1$  and  $i_1$  can now be used in the place of  $K$  and  $i_\infty$  in the equations from section III.A to compute the position and velocity vectors for the first impulse. The magnitude of the second impulse can also be computed using the trigonometric relation

$$\frac{\Delta V_2}{V_{circ}} = \sqrt{K^2 + K_1^2 \sin^2(\varphi)} - K_1 \sin(\varphi) \quad (51)$$

This relation requires  $\varphi < \frac{\pi}{2}$ , but this is always the case for optimal solutions. The angle  $\varphi$  is given by

$$\cos(\varphi) = \frac{V_{circ}}{\Delta V_1} \left( K_1 - w \sqrt{\frac{1 + K_1 w - w^2}{2 + K_1 w}} \right) \quad (52)$$

Finally, the angle  $i_2$  can now be found using

$$i_2 = \varphi - \sin^{-1} \left[ \frac{K_1}{K} \sin(\varphi) \right] \quad (53)$$

The above equations must be used to solve for  $K_1$  as a function of  $K$  and  $i_\infty$  numerically. This is done by adjusting the value of  $K_1$  with a method such as the secant method until  $i_1 + i_2$  reaches the desired value  $i_\infty$ . An effective strategy for producing initial guesses to start the numerical iteration is given by the approximation

$$K_1 \approx \left( 1 - \frac{2}{\pi} i_\infty \right) K \quad (54)$$

Note that when the resulting  $K_1$  is greater than  $K$  a single-impulse maneuver will consume less fuel than the double-impulse maneuver. Optimal values for  $K_1$  are shown as a function of  $K$  and  $i_\infty$  in figure 7.

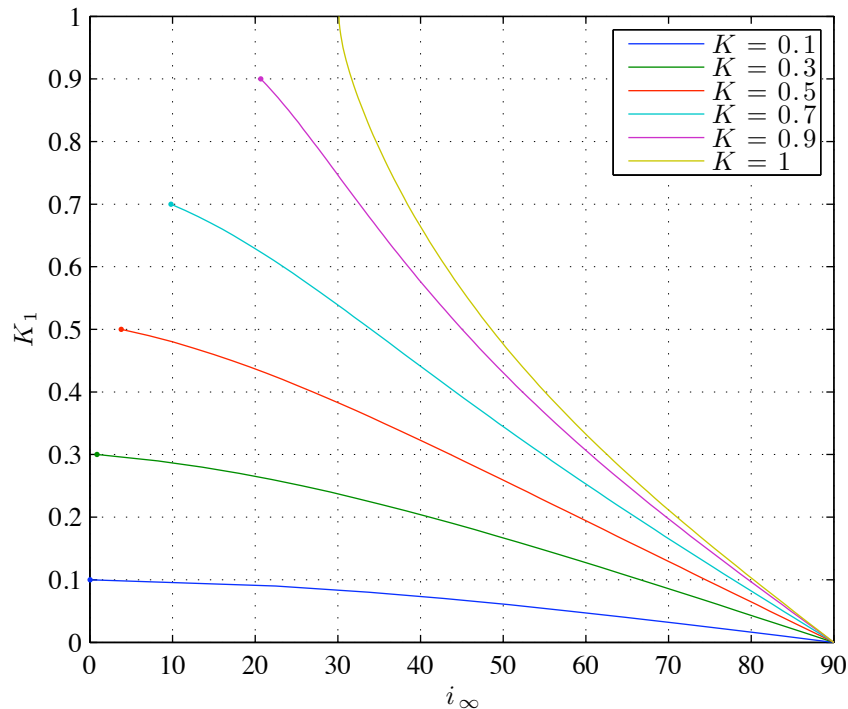


**Figure 7.**  $K_1$  as a function of  $K$  and  $i_\infty$ . The lines terminate when  $K_1 = K$ . Beyond this point a single burn maneuver is the minimum total impulse solution.

Figure 8 shows the total  $\Delta V$  for the double-impulse maneuver. The magnitude of the single-impulse maneuver is also shown.

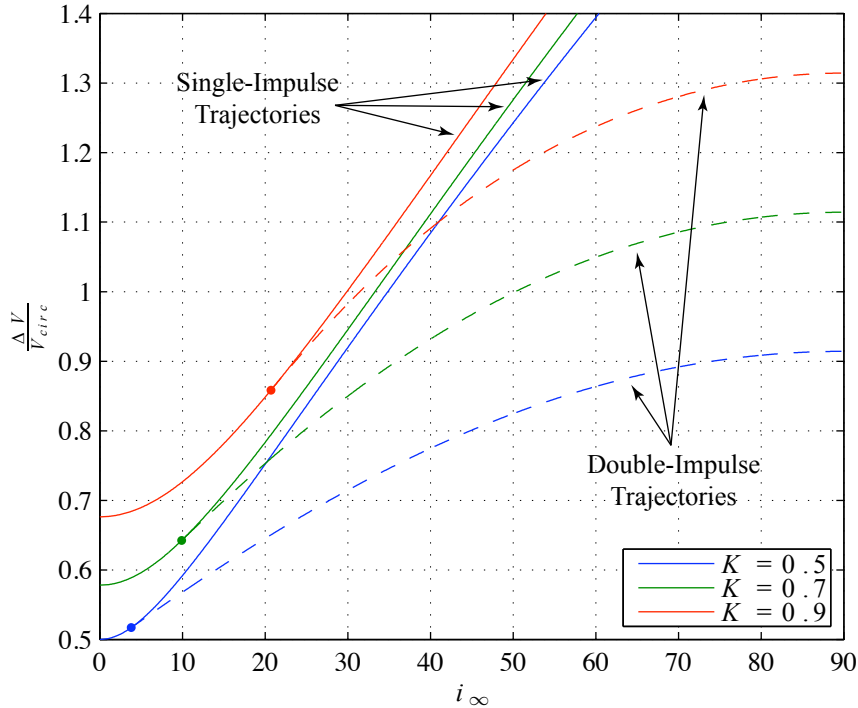


Figure 8. The  $\Delta V$  cost for a single-impulse maneuver is shown with a solid line. While the  $\Delta V$  cost of the two-impulse maneuver is shown with the dashed line.

### III.C. Triple-Impulse Maneuver

Although the double-impulse maneuver offers substantial fuel savings, especially for larger values of  $i_\infty$ , a three impulse maneuver can be designed that requires even less fuel than the two impulse maneuver. The geometry of the three-impulse maneuver is shown in Figure 9. The primary purpose of the first impulse is to boost the orbital energy of the craft. Some fuel savings are achieved by performing a small fraction of the total required plane change with the first impulse. The first impulse places apoapsis of the orbit at the intersection of the current orbital plane and the plane containing the hyperbolic escape with the minimal dihedral angle. The only purpose of the second impulse is to change the orbital plane so that the resulting orbital plane includes the escape asymptote. The third impulse then boosts the orbital energy and places the spacecraft on the desired escape asymptote.

The approach outlined in this section is loosely based on a technique presented by Webb.<sup>5,6</sup> The strength of the triple-impulse maneuver is the substantial reduction in  $\Delta V$  required to execute the required maneuver. However, the disadvantage of this maneuver is that it requires a substantially longer time of flight to reach to sphere of influence. Although not fuel-optimal,<sup>13</sup> this algorithm attempts to minimize the time of flight required by consuming all of the budgeted fuel. This technique is not a fuel-optimal technique.

The motivation for the three-impulse technique is to perform the majority of the required plane change relatively far away from the central body, and boost the orbital energy as near the central body as possible. This significantly reduces the  $\Delta V$  consumed by the plane change portion of the maneuver, but maximizes the orbital energy gains. In this paper the magnitude of the plane change is minimized by constraining the position vectors of the impulses used to execute the plane change to be orthogonal to the escape asymptote. The dihedral angle of the plane change is then simply  $i_\infty$ .

The triple-impulse maneuver can be viewed as a two part maneuver. The first two impulses execute a plane change while the third impulse performs the injection from a bounded elliptic orbit to a hyperbolic escape orbit.

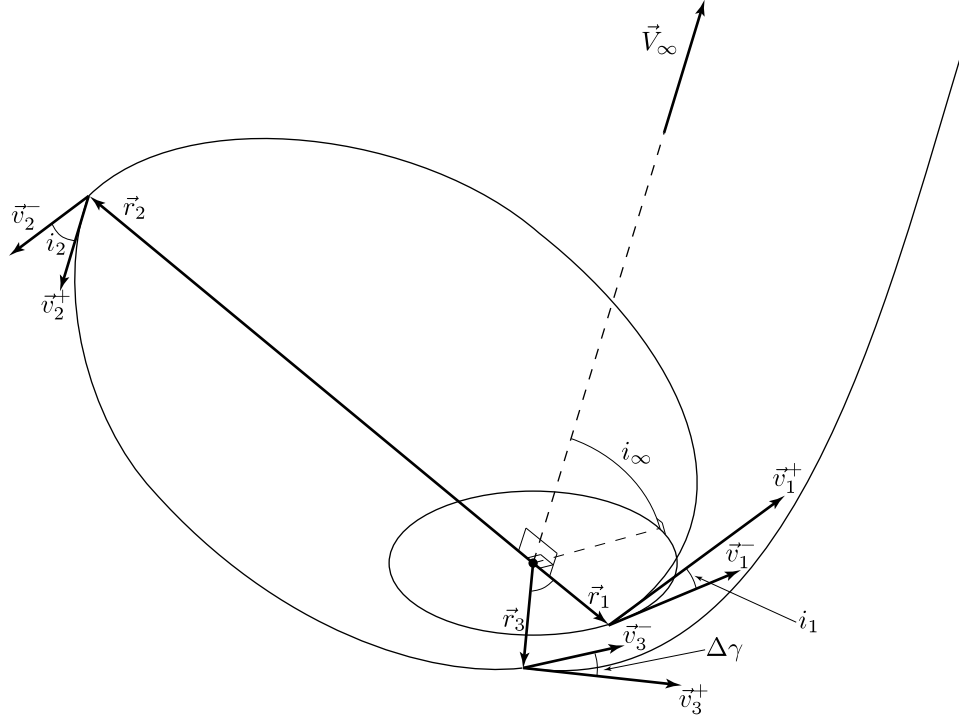


Figure 9. The geometry of the three-impulse maneuver. The first impulse occurs at the periapse of a high-energy elliptic orbit. The second impulse occurs near at apoapsis of the transfer ellipse and the majority of the plane change portion of the maneuver. The third maneuver occurs near periapse of the final hyperbolic escape trajectory.

### III.C.1. The first impulse

The primary purpose of the first impulse is to place the spacecraft on an elliptic transfer orbit, by raising the orbital energy. Therefore this impulse is performed at the periapse of the desired transfer orbit, and has no radial component. By including a small fraction,  $i_1$ , of the total plane change,  $i_\infty$ , in this impulse some fuel savings can be achieved without significant computational effort.

### III.C.2. The second impulse

The second impulse is performed at apoapsis of the transfer ellipse where the orbital velocity is lowest. The only objective of the second impulse is to realize the vast majority of the needed plane change, which was not included in the first impulse. This impulse does not alter the energy of the orbit or the eccentricity of the the elliptic transfer orbit. This maneuver is a pure plane change, and does not have any net effect on the radial or transfers components of velocity.

Webb presents an equation for calculating the optimal distribution of the plane change between the first two impulses

$$f(i_1) = \frac{V_p V_{circ} \sin(i_1)}{\Delta V_1} - V_a \cos\left(\frac{i_\infty - i_1}{2}\right) = 0 \quad (55)$$

where  $\Delta V_1$ ,  $V_p$  and  $V_a$  are magnitude of the first impulse, and the velocities at periapse and apoapsis of the transfer ellipse respectively. These values are calculated with the vis-viva integral, the law of cosines and  $a_e$ ,

the semi-major axis of the transfer orbit.

$$\Delta V_1^2 = V_p^2 + V_{circ}^2 - 2V_p V_{circ} \cos(i_1) \quad (56)$$

$$V_p^2 = \mu_m \left( \frac{2}{r_{circ}} - \frac{1}{a_e} \right) \quad (57)$$

$$V_a^2 = \mu_m \left( \frac{2}{2a_e - r_{circ}} - \frac{1}{a_e} \right) \quad (58)$$

Note that all of the values used to calculate the first two impulses are known quantities except for  $a_e$ .

Equation 55 is implicit in  $i_1$  and must be solved numerically. A Newton-Raphson iterations works well but requires the derivative of equation 55 with respect to  $i_1$

$$\frac{df(i_1)}{di_1} = \frac{V_p V_{circ}}{\Delta V_1} \left[ \cos(i_1) - \frac{V_p V_{circ} \sin^2(i_1)}{\Delta V_1^2} \right] + \frac{\Delta V_2}{4} \quad (59)$$

where  $\Delta V_2$  is given by

$$\Delta V_2 = 2V_a \sin\left(\frac{i_\infty - i_1}{2}\right) \quad (60)$$

For this problem an excellent starting guess that will insure rapid convergence is 0.03 rad. The magnitude of the plane change for the second impulse is found through subtraction.

$$i_2 = i_\infty - i_1 \quad (61)$$

### III.C.3. The third impulse

The third impulse transfers the spacecraft from the elliptic transfer orbit to a hyperbolic orbit with the desired escape asymptote. A procedure can be developed of finding the magnitude for this impulse as a function of the true anomaly of the elliptic transfer orbit. The required numeric optimization is quickly accomplished.

Begin by noting that when,  $f_e$ , the true anomaly of the return leg of the transfer ellipse is  $\frac{\pi}{2}$ , the radial vector is pointing in the direction of the escape asymptote. The conic equation for a hyperbola with this departure asymptote can be written directly in terms of  $f_e$ , the true anomaly of the ellipse,

$$r_h = \frac{\mu_m}{V_\infty^2} \frac{e_h^2 - 1}{1 - \sin(f_e) + \sqrt{e_h^2 - 1} \cos(f_e)} \quad (62)$$

where the subscripts indicate whether the classical orbital elements correspond to the elliptic or hyperbolic trajectories. The flight path angle can also be written as a function of  $f_e$

$$\tan(\gamma_h) = \frac{\cos(f_e) + \sqrt{e_h^2 - 1} \sin(f_e)}{1 - \sin(f_e) + \sqrt{e_h^2 - 1} \cos(f_e)} \quad (63)$$

The equivalent equations for the elliptic orbit are well known

$$r_e = a_e \frac{1 - e_e^2}{1 + e_e \cos(f_e)} \quad (64)$$

$$\tan(\gamma_e) = \frac{e_e \sin(f_e)}{1 + e_e \cos(f_e)} \quad (65)$$

The eccentricity of the elliptic transfer orbit is given by

$$e_e = 1 - \frac{r_{circ}}{a_e} \quad (66)$$

If equation 62 is solved for  $e_h$  it results in a quadratic equation with only one positive real root.

$$e_h^2 = \frac{1}{4} \left( \frac{r_h V_\infty^2}{\mu_m} \cos(f_e) + \sqrt{\frac{r_h^2 V_\infty^4}{\mu_m^2} \cos^2(f_e) + 4 \frac{r_h V_\infty^2}{\mu_m} [1 - \sin(f_e)]} \right)^2 + 1 \quad (67)$$

The hyperbolic eccentricity can be found by equating the radial distances,  $r_h = r_e$ , where  $r_e$  is the radial distance at  $f_e$ . Next,  $\gamma_e$  can be computed by using equation 65. The change in the flight path angle executed during the maneuver can now be found

$$\Delta\gamma = \gamma_h - \gamma_e \quad (68)$$

If  $\Delta\gamma$  becomes negative, the possibility for lunar impact exists. Should this occur,  $\Delta\gamma$  is set equal to zero. Equations 62 and 63 are set equal to equations 64 and 65, and the resulting two expressions are solved simultaneously for  $e_h$  and  $f_e$ . However, this situation has not yet been encountered.

With this angle the magnitude of the maneuver can now be computed using the law of cosines

$$\Delta V_3^2 = V_e^2 + V_h^2 - 2V_e V_h \cos(\Delta\gamma) \quad (69)$$

where vis-viva integral is used to find the needed velocities

$$V_e^2 = \mu_m \left( \frac{2}{r} - \frac{1}{a_e} \right) \quad (70)$$

$$V_h^2 = 2\frac{\mu_m}{r} + V_\infty^2 \quad (71)$$

The value of  $f_e$  that minimizes the the sum of the  $\Delta V$  can now quickly be found through the use of numerical optimization methods. Examples of the curves that are minimized are shown in figure 10.

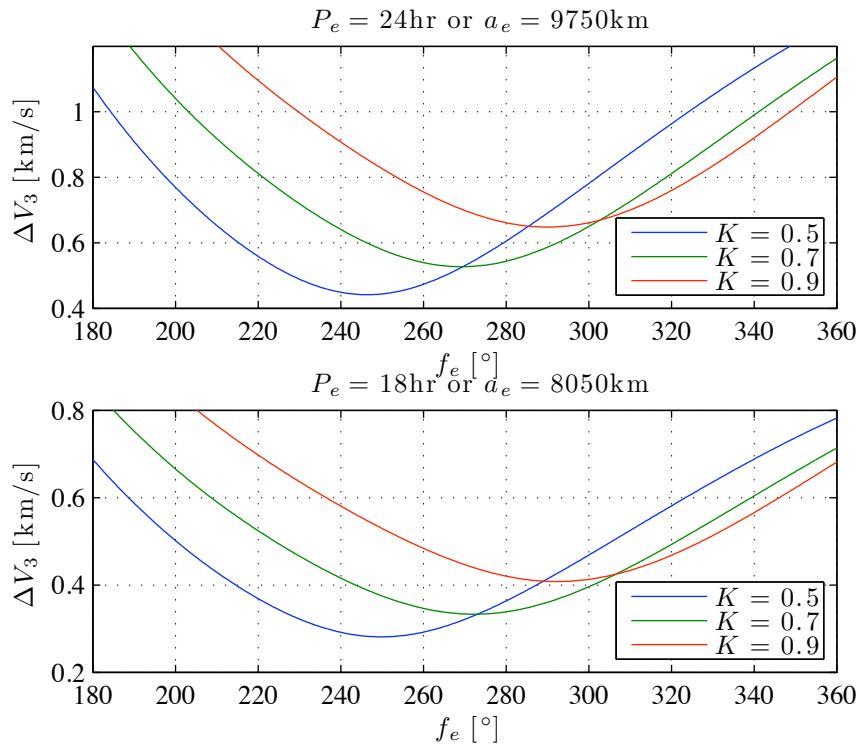


Figure 10. The magnitude of the third burn as a function of location. For these charts  $i_\infty = 70^\circ$ .

#### III.C.4. Selecting $a_e$

At this point the position and velocity vectors needed define all of impulsive maneuvers can easily be computed. Additionally, all of the parameters for the three-impulse maneuver are known as a function of  $a_e$ . Both the impulsive cost of the maneuver sequence and the length of time spent on the transfer trajectories are functions of  $a_e$ . The partial derivative of  $\Delta V$  with respect to  $a_e$  is negative, meaning that, as  $a_e$  is increased the  $\Delta V$  required to execute the impulsive sequence decreases. Meanwhile, the partial derivative

of the period of the ellipse with respect to its semimajor axis is negative; meaning that the time required to traverse the elliptic legs of the trajectory increases with  $a_e$ .

The strategy employed to select  $a_e$  is simply to decrease the value of  $a_e$  until all of the  $\Delta V$  capacity budgeted for the maneuver is utilized by the impulsive sequence. The principle advantages to this approach is the shorter time of flight required to execute the sequence achieved by minimizing the time spent traversing the transfer ellipse. The consumption of all the budgeted fuel is justified by the fact that any fuel that is saved will ultimately be disposed of upon returning to Earth. If this technique were used to compute a lunar orbit injection sequence rather than a return sequence it may be advantageous to simply choose a value for  $a_e$  that fulfills mission objectives. However, for the return journey minimizing the flight time has an attractive effect on the probability of mission success.<sup>10</sup> As always, sound engineering judgment should govern the method used to select  $a_e$ .

The results of some example calculations are shown in figure 11. These values were computed by assuming a circular 100 km circular lunar orbit, with  $K = 0.625$ .

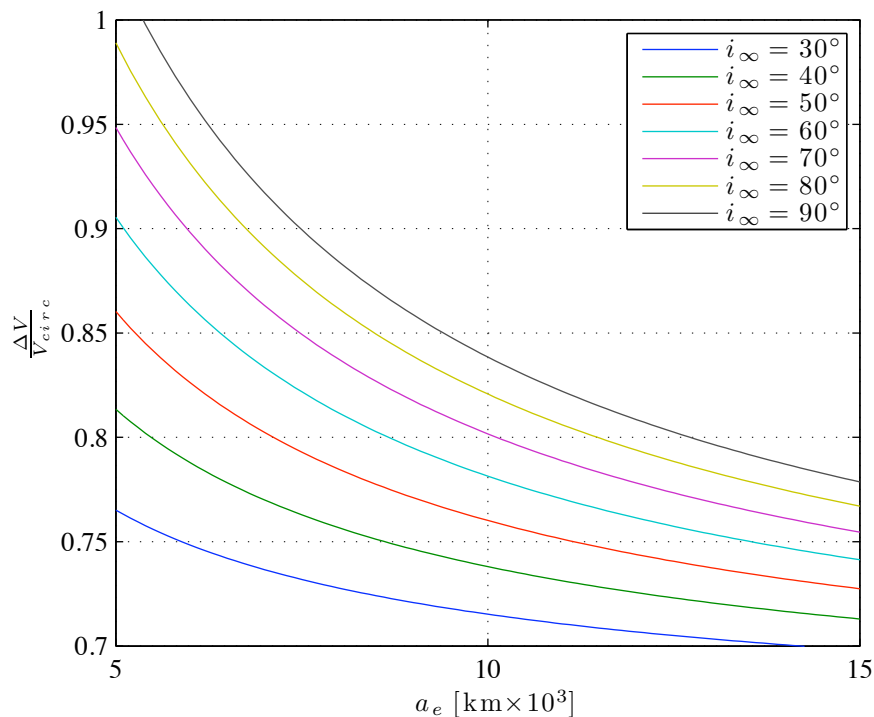


Figure 11. The total impulsive cost of a three-impulse sequence. For this plot  $K = 0.625$  and  $r_{circ} = 1837$  km.

### III.D. Selecting the Number of Impulses

Minimizing the number of impulses is accomplished by first computing the needed  $\Delta V$  to perform the single-impulse maneuver. If this does not exceed the capacity of the spacecraft the single-impulse maneuver is performed. Should the fuel available be insufficient to execute the single-impulse maneuver, the fuel required to complete the double-impulse sequence is computed. If the fuel needed to perform this maneuver is available then this maneuver is executed. If there is not enough fuel to support the single- or double-impulse maneuvers, the triple-impulse maneuver that consumes all of the available fuel, and minimize the period of the transfer ellipse is computed. The overall procedure has the effect of minimizing the number of impulses and keeping the transfer time to a minimum.

### III.E. Correcting the $t_{SoI}$

When the  $\vec{V}_{SoI}$  was generated it was associated with an epoch,  $t_{SoI}$ , which is the anticipated epoch when the SoI will be pierced. Since the injection sequence was computed using this escape asymptote it is associated with the same epoch. This means that the spacecraft must arrive at the position of first impulse of the injection sequence at precisely the specified time. However, the arrival time of the spacecraft at the initial impulse can only be controlled by moving the location of the impulse, which in turn can only be controlled by adjusting  $t_{SoI}$  or  $t_{FR}$ . This problem can be rapidly resolved by adjusting  $t_{SoI}$  with a relatively simple iterative procedure.

First, the time-of-flight for the hyperbolic trajectory is computed. Kepler's equation for hyperbolic orbits can be used to find the time of flight as a function of the radial distances at the ends of the trajectory, and  $V_\infty$ . The hyperbolic anomaly can be expressed as a function of the radial distance,  $r$ , at some point and  $V_\infty$ .

$$\cosh(H) = \frac{1}{e_h} \left[ 1 + \frac{rV_\infty^2}{\mu_m} \right] \quad (72)$$

Some attention must be given to the quadrant ambiguity in  $H$ . At the sphere of influence  $H_{SoI} > 0$ . The single- and double-impulse cases require that the transfer from the circular to the hyperbolic orbit occur after the hyperbolic periapse, meaning that  $H_t > 0$ . For the hyperbolic leg of the three impulse maneuver the transfer can (and frequently does) occur before periapse. The sign of  $H_t$  should then be the same as the sign of,  $\gamma_h$ , the flight path angle at the same point. The time of flight needed for the hyperbolic leg of the trajectory can now be computed with Kepler's equation.

$$t_h = \frac{\mu_m}{V_\infty^3} [e_h \sinh(H_{SoI}) - H_{SoI} - e_h \sinh(H_t) + H_t] \quad (73)$$

The time of flight required for the elliptic transfer arcs is computed using a similar method

$$\cos(E_t) = 2\pi - \frac{1}{e_e} \left[ 1 - \frac{r_t}{a_e} \right] \quad (74)$$

The  $2\pi$  resolves the quadrant ambiguity by assuring  $E_t$  is always a reflex angle. The elliptic time-of-flight,  $t_e$ , is given by Kepler's equation

$$t_e = \sqrt{\frac{a_e^3}{\mu_m}} [E_t - e_e \sin(E_t)] \quad (75)$$

Finally, the time required for the spacecraft to arrive at the location of the first impulse is computed. The position of the spacecraft on the circular orbit is computed at  $t_{SoI} - t_h - t_e$ . The central angle of the arc that the spacecraft must travel to arrive at the location of the first impulse can be used to find the time required to arrive there.

$$t_c = \sqrt{\frac{r_{circ}^3}{\mu_m}} \Delta f_c \quad (76)$$

The first time this value is computed  $\Delta f_c$  should be a positive value. However, subsequent calculations of this angle can be positive or negative. It is important to note that only the first value of  $\Delta f_c$  is allowed to be reflex. By mandating that the first value of  $t_c$  be positive it is assured that the net change in  $t_{SoI}$  will be positive. Note that largest possible value for  $t_c$  is less than the period of the circular lunar orbit ( $\sim 2$  hrs).

The epoch where the SoI is pierced can now be corrected.

$$t_{SoI}^+ = t_{SoI}^- + t_c \quad (77)$$

The  $\vec{V}_\infty$  vector can now be found for the new epoch and the injection sequence can be recomputed. For the relatively small values of  $t_c$ ,  $\vec{V}_\infty$  only experiences relatively minor changes. Consequently the changes in the injection sequence are also very small. The relatively static behavior of  $\vec{V}_\infty$  allows  $t_c$  to vanish within just a few iterations.

## IV. Differential Trajectory Correction

The initial estimate of the TEI maneuvers places the spacecraft on a hyperbolic asymptote with the correct velocity, but not the correct position (i.e.  $\vec{r}_T$  is not on the hyperbolic escape asymptote). The gravity focusing effect of the Earth helps to nullify the effect of this disconnect, but the residual must be removed. The initial estimates also need to be corrected for trajectory dispersions due to the non-Keplerian gravity field inside the SoI. These corrections can also remove the effects of smaller forces that have not been considered up to this point such as spherical harmonic gravity fields, and atmospheric drag. The techniques used to perform this correction are the same techniques that are used to compute fixed-time of arrival trajectory correction maneuvers (TCMs). Thus a working version of the required software should already be onboard the spacecraft.

Battin<sup>11</sup> gives a technique for fixed-time lunar targeting which will be outlined here. This method is easily extended to facilitate the desired targets through the process of linearization.

Given a nominal trajectory,  $\bar{\mathbf{x}}(t)$ , a linear system can be obtained by taking the partials of the dynamics and evaluating them along the nominal trajectory. This paper will only consider conservative systems, which can be expressed as potential function (such as gravity). For a conservative system the dynamics partials are given by

$$\left. \frac{\partial \dot{\mathbf{x}}}{\partial \mathbf{x}} \right|_{\bar{\mathbf{x}}}(t) = \begin{bmatrix} \mathbf{0}_{3 \times 3} & \mathbf{I}_{3 \times 3} \\ \mathbf{G}(t) & \mathbf{0}_{3 \times 3} \end{bmatrix} \quad (78)$$

Non-conservative systems can also be modeled by including the appropriate partial in the bottom right hand block.  $\mathbf{G}(t)$  is the Hessian of the potential function with respect to the position. The differential equation for the linearized state transition matrix,  $\Phi$ , can now be written as

$$\dot{\Phi}(t, t_0) = \begin{bmatrix} \mathbf{0}_{3 \times 3} & \mathbf{I}_{3 \times 3} \\ \mathbf{G}(t) & \mathbf{0}_{3 \times 3} \end{bmatrix} \Phi(t, t_0) \quad (79)$$

subject to the initial condition  $\Phi(t_o, t_o) = \mathbf{I}_{6 \times 6}$ . This equation can be integrated to yield the linearized state transition matrix relating the initial state to the final state.

$$\Phi(t, t_0) = \left. \frac{\partial \mathbf{x}(t)}{\partial \mathbf{x}(t_0)} \right|_{\bar{\mathbf{x}}} = \begin{bmatrix} \Phi_{rr} & \Phi_{rv} \\ \Phi_{vr} & \Phi_{vv} \end{bmatrix} \quad (80)$$

The desired targets at atmospheric entry interface are

$$\mathcal{T}_i(t_i) = \begin{bmatrix} i_R \\ \gamma_i \\ r_i \end{bmatrix} \quad (81)$$

For the intermediate burns the targets are simply the position vector for the next impulse.

$$\mathcal{T}_n = \vec{r}_{n+1}$$

The partials of the final targets in equation 81 are taken with respect to the state vector

$$\frac{\partial \mathcal{T}_i}{\partial \mathbf{x}} = \begin{bmatrix} \frac{-1}{\sin(i_R)h_i} \begin{bmatrix} 0 & 0 & 1 \end{bmatrix} \left( \mathbf{I} - \hat{i}_{\vec{h}_i} \hat{i}_{\vec{h}_i}^T \right) \begin{bmatrix} -[\vec{v}_i \times] & [\vec{r}_i \times] \end{bmatrix} \\ \frac{1}{\cos(\gamma_i)} \begin{bmatrix} \hat{i}_{\vec{v}_i}^T \\ r_i \end{bmatrix} \left( \mathbf{I} - \hat{i}_{\vec{r}_i} \hat{i}_{\vec{r}_i}^T \right) \begin{bmatrix} \hat{i}_{\vec{r}_i}^T \\ v_i \end{bmatrix} \left( \mathbf{I} - \hat{i}_{\vec{v}_i} \hat{i}_{\vec{v}_i}^T \right) \\ \begin{bmatrix} \hat{i}_{\vec{r}_i}^T \\ \mathbf{0}_{1 \times 3} \end{bmatrix} \end{bmatrix} \quad (82)$$

where  $\hat{i}$  a unit vector with respect to its subscript,  $[\cdot \times]$  indicates the crossproduct matrix, and  $\vec{h}_i = \vec{r}_i \times \vec{v}_i$ . The partials for the intermediate target vectors are simply

$$\frac{\partial \mathcal{T}_n}{\partial \mathbf{x}} = \begin{bmatrix} \mathbf{I}_{3 \times 3} & \mathbf{0}_{3 \times 3} \end{bmatrix} \quad (83)$$

Linear system theory allows for the computation of an impulsive maneuver that will correct a small defect in the the targeted state,  $\delta\mathcal{T}(t)$ , thus causing the trajectory to meet all the target constraints at the targeted time,  $t$ .

$$-\delta\mathcal{T}(t) = \frac{\partial\mathcal{T}}{\partial\mathbf{x}}\bigg|_t \Phi(t, t_0) \begin{bmatrix} \mathbf{0}_{3\times 1} \\ \delta\Delta\vec{V} \end{bmatrix} \quad (84)$$

This equation is solved for the correction to the impulse

$$\delta\Delta\vec{V} = -\mathbf{M}^{-1}\delta\mathcal{T}(t) \quad (85)$$

where

$$\mathbf{M} = \frac{\partial\mathcal{T}}{\partial\mathbf{x}}\bigg|_t \begin{bmatrix} \Phi_{rv}(t, t_0) \\ \Phi_{vv}(t, t_0) \end{bmatrix} \quad (86)$$

By repeating this procedure, the magnitude of  $\delta\mathcal{T}$  vanishes, quickly removing the effects of nonlinearities, and producing the final solution.

## V. Results

An example of these calculations for a 100 km circular orbit and 1.5 km/s of  $\Delta V$  capacity is shown in figure 12. This figure shows the number of impulses and the time-of-flight to reach the Sol as a function of  $K$  and  $i_\infty$ .

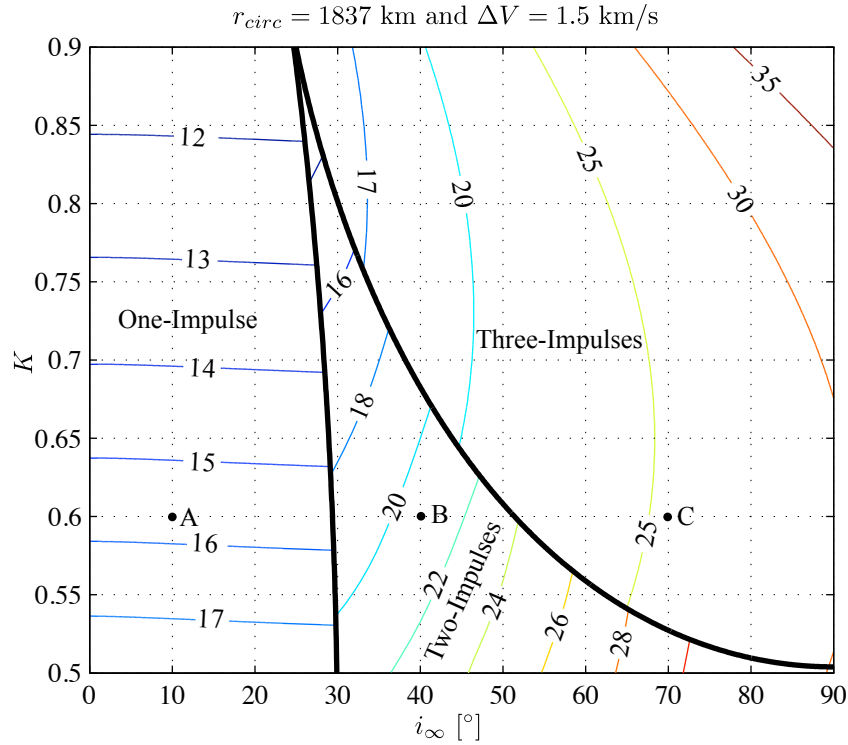


Figure 12. Regions showing the number of required impulses. The contours represent the time-of-flight from the first impulse to the time when the spacecraft reaches the Sol in hours.

Three example cases were selected to demonstrate the procedure. The values for all three cases were computed using the same epoch for  $t_{Sol}^d$  and the same value for  $t_{FR}$ . The time corrections discussed in section III.E were also omitted from these calculations to enable the same  $\vec{V}_{Sol}$  to be used for each case. The values used to compute  $\vec{V}_{Sol}$  are shown in table 1.

<sup>d</sup>All epochs are in seconds past 1 January 2000 12:00:00 UTC (J2000).

Table 1. Orbital parameters for the trans-earth trajectory used in the examples. This trajectory has an atmospheric entry from the south to north. The epoch for  $t_{SoI}$  is 14 July 2009 00:00:00.00 UTC.

Parameter	Value
$t_{SoI}$	300801666.183748 s
$t_{FR}$	2.828 days
$t_i$	301046005.383748 s
$r_{SoI}$	66,000 km
$i_R$	40°
$\gamma_i$	-6°
$r_i$	6500 km
$\left(\vec{V}_{SoI}\right)_x$	-0.516 km/s
$\left(\vec{V}_{SoI}\right)_y$	-0.719 km/s
$\left(\vec{V}_{SoI}\right)_z$	-0.588 km/s
$\left(\vec{V}_\infty\right)_x$	-0.477 km/s
$\left(\vec{V}_\infty\right)_y$	-0.663 km/s
$\left(\vec{V}_\infty\right)_z$	-0.543 km/s
$r_{circ}$	1837 km
$K$	0.6

For this analysis the escape energy is fixed. Different cases must then be generated by varying  $i_\infty$ . This is accomplished by selecting an appropriate unit normal vector. The unit normal vectors that were selected are shown in table 2

Case A is a single-impulse maneuver. Differential correction was used remove the effect of all non-Keplerian forces acting on the body, and enforce the boundary conditions. The results of these calculations are shown in table 3. For case A 1.002 km/s of  $\Delta V$  was predicted. After correction, the single impulse consumed 0.989 km/s of  $\Delta V$ .

Case B is a double-impulse maneuver. Differential correction was used remove the effect of all non-Keplerian forces acting on the body, and enforce the conditions at atmospheric interface. The initial estimate of the first impulse produced a position error due to non-Keplerian gravity at the epoch of the second impulse of nearly 500 km. Since the desired position was arbitrarily placed near the SoI, this error was ignored and no correction was applied to the initial impulse. Differential correction was used on the final impulse to enforce the boundary conditions at atmospheric interface. Table 4 shows the results of these calculations. Before correction it was predicted that 1.377 km/s of  $\Delta V$  would be used. After the final impulse was corrected, nearly 1.669 km/s of  $\Delta V$  was required to complete the maneuver. This rather substantial error is due to the approximation of an infinite radial distance with the radius of the SoI. Possible strategies for decreasing the magnitude of this error are presented in the next section.

Case C is a triple-impulse maneuver. Like the double-impulse maneuver corrections to the first two impulses were ignored. The cumulative position error caused by non-Keplerian gravity at the epoch of the third impulse is less than 20km. Thus the relatively minor corrections to these two impulses were neglected. Applying a linear differential correction to the final impulse can lead to numerical instabilities. These instabilities are caused by the position vector of the impulse being nearly 180° from the escape asymptote. This difficulty is avoided by placing a trajectory correction maneuver at point where the spacecraft pierces the lunar sphere of influence. This corrective maneuver had a magnitude of 30 m/s, and the final cost of the maneuver was 1.530 km/s.

**Table 2. Parameters for the lunar orbits.**

Case	$r_{circ}$ [km]	$\hat{i}_{\vec{h}}$	$i_{\infty}$
A	1837	-0.934966	10°
		0.344325	
		0.085313	
B	1837	-0.981018	40°
		-0.124668	
		-0.148532	
C	1837	-0.743650	70°
		-0.571825	
		-0.346411	

## VI. Further Work

Several areas have been identified for possible improvement of the procedures outlined in this paper.

### VI.A. Generating the $\vec{V}_{\infty}$

The time required to calculate  $\vec{V}_{\infty}$  is entirely a function of the time required to perform the needed trajectory integrations. An alternative method might be developed where a set (or range) of  $\vec{V}_{\infty}$  vectors would be generated for each epoch and time-of-flight. The boundary conditions at the Earth would not be fixed, but simply constrained to acceptable intervals. The algorithm would then pick the the  $\vec{V}_{\infty}$  that minimizes  $i_{\infty}$ . Alternatively, the total time-of-flight could be minimized.

### VI.B. Computing the impulses

The  $\Delta V$  requirements for the three-impulse maneuver can be further reduced by adding an additional degree of freedom to the optimization. This can be accomplished by relaxing the constraint that maintains the line of nodes for the ellipse perpendicular to the escape asymptote. Such a technique will decrease the fuel consumed without substantial increase in the computational cost.

Experience has shown that the third impulse of a three-impulse maneuver always occurs at the second intersection of the trajectories. It should be possible to prove that this will always be the global minimum.

More accurate estimates of the two-impulse maneuver can be computed by introducing a velocity correction to the second impulse. This can be accomplished by replacing  $K$  and  $K_1$  in equation 51 with values that reflect the velocity at the SoI rather than the velocity at an infinite radial distance. This will result in a sub-optimal maneuver, but will remove a substantial portion fuel estimate error.

### VI.C. Differential Correction

Gravity focusing causes the altitude and crosstrack errors at reentry to be relatively minor. However, the downrange error is magnified. A variable time-of-flight targeting scheme can reduce these large downrange errors without adding substantial  $\Delta V$ . Such a targeting strategy may allow for substantial reduction in the magnitude of the required correction.

## VII. Summary

This paper presents a relatively simple and robust technique for computing a TEI maneuver that minimizes the number of impulses required for an earth return from a circular lunar orbit subject to a fuel constraint and, in the case of a 3-impulse solution, minimizes the time-of-flight. This has been achieved by

**Table 3. Detailed information for the single-impulse maneuver.**

$j$	Epoch [s]	$(r_{\vec{M}})_j$ [km]	Uncorrected Values		Corrected Values	
			$(\vec{v}_M)_j^-$ [km/s]	$(\vec{v}_M)_j^+$ [km/s]	$(\vec{v}_M)_j^-$ [km/s]	$(\vec{v}_M)_j^+$ [km/s]
1	300745287.394293	580.290	-0.263690	-0.862193	-0.263690	-0.834271
		1685.575	-0.324721	-0.114228	-0.324721	-0.152428
		-443.473	-1.579256	-2.354251	-1.579256	-2.368699

**Table 4. Detailed information for the double-impulse maneuver.**

$j$	Epoch [s]	$(r_{\vec{M}})_j$ [km]	Uncorrected Values		Corrected Values	
			$(\vec{v}_M)_j^-$ [km/s]	$(\vec{v}_M)_j^+$ [km/s]	$(\vec{v}_M)_j^-$ [km/s]	$(\vec{v}_M)_j^+$ [km/s]
1	300725815.209580	-262.188	0.214465	0.168278	-	-
		1805.261	0.223494	0.335990	-	-
		216.469	-1.604083	-2.363210	-	-
2	300801666.183748	10411.558	0.116786	-0.475857	0.116786	-0.762351
		-47420.691	-0.569556	-0.663242	-0.569556	-0.719979
		-44708.808	-0.445486	-0.542715	-0.445486	-0.565222

**Table 5. Detailed information for the triple-impulse maneuver.**

$j$	Epoch [s]	$(r_{\vec{M}})_j$ [km]	Uncorrected Values		Corrected Values	
			$(\vec{v}_M)_j^-$ [km/s]	$(\vec{v}_M)_j^+$ [km/s]	$(\vec{v}_M)_j^-$ [km/s]	$(\vec{v}_M)_j^+$ [km/s]
1	300709941.952098	-441.573	1.019213	1.233569	-	-
		1308.261	-0.665277	-0.916607	-	-
		-1211.625	-1.089787	-1.439284	-	-
2	300727843.422705	2164.001	-0.251715	0.208573	-	-
		-6411.344	0.187037	0.290706	-	-
		5937.764	0.293692	0.237878	-	-
3	300743731.88287	1484.166	-0.710453	-0.905999	-	-
		2063.220	0.337225	0.614344	-	-
		1694.676	-1.298829	-1.724149	-	-
TCM		-33510.836	-	-	-0.526943	-0.509188
		-40512.388	-	-	-0.701687	-0.724606
		-39811.718	-	-	-0.577319	-0.584732

modifying, extending, and integrating several well known and documented techniques from the Apollo era. The result is a prototype TEI maneuver algorithm that can be used at any time for any circular lunar departure orbit. The convergence properties of the algorithm are intuitive and robust, and memory requirements are minimal. The algorithm may be well suited for abort and contingency operations when CPU is at a premium or when for initializing more complex optimization routines.

## References

- <sup>1</sup>Edelbaum, T. N., "Optimal Nonplanar Escape from Circular Orbit," *AIAA Journal*, Vol. 9, No. 9, December 1971, pp. 2432–2436.
- <sup>2</sup>Pu, C. L. and Edelbaum, T. N., "Four-Body Trajectory Optimization," *AIAA Journal*, Vol. 13, No. 3, March 1975, pp. 333–336.
- <sup>3</sup>Gunther, P., "Asymptotically Optimum Two-Impulse Transfer from Lunar Orbit," *AIAA Journal*, Vol. 4, No. 2, February 1966, pp. 346–352.
- <sup>4</sup>Kitchens, M. D., Messer, C. W., and Bristow, R. B., "A Preliminary Evaluation of Apollo Capabilities for Lunar Orbit Coverage and Lunar Surface Landings Utilizing Multiple-Impulse Techniques for TransEarth Injection from Highly Inclined Lunar Orbits," NASA Program Apollo Working Paper No. 1199 TMX-65201, NASA Manned Spacecraft Center, Houston, Texas, April 1966.
- <sup>5</sup>Webb, E. D., "A Preliminary Analysis of a Three-Impulse Technique for Transearth Injection from Highly Inclined Orbits," Tech. Rep. LMSC/A822605, Lockheed Missiles and Space Company, Sunnyvale, California, May 1966.
- <sup>6</sup>Webb, E. D., "Three-Impulse Transfer from Lunar Orbits," *Space Flight Mechanics Specialist Symposium*, No. AAS 66-134, American Astronautical Society, July 1966.
- <sup>7</sup>Bean, W. C., "Minimum Delta V, Three-Impulse Transfer onto a Trans-Mars Asymptotic Velocity Vector," NASA Technical Note TN D-5757, Manned Spacecraft Center, Houston, Texas 77058, April 1970.
- <sup>8</sup>Jezewski, D. J. and Rozendaal, H. L., "An Efficient Method for Calculating Optimal Free-Space N-Impulse Trajectories," *AIAA Journal*, Vol. 6, No. 11, November 1968, pp. 2160–2165.
- <sup>9</sup>Marchand, B. G., Howell, K. C., and Wilson, R. S., "An Improved Corrections Process for Constrained Trajectory Design in the n-Body Problem," unpublished document.
- <sup>10</sup>Roche, R., "Selection of the Optimum Abort Trajectory," Apollo Guidance and Navigation Note 71, Bissett-Berman Corp., May 1963.
- <sup>11</sup>Battin, R. H., *An Introduction to the Mathematics and Methods of Astrodynamics*, American Institute of Aeronautics and Astronautics, 1999.
- <sup>12</sup>Bate, R. R., Mueller, D. D., and White, J. E., *Fundamentals of Astrodynamics*, Dover Publications, 1971.
- <sup>13</sup>Gerbracht, R. J. and Penzo, P. A., "Optimum Three-Impulse Transfer Between an Elliptic Orbit and a non Coplanar Escape Asymptote," *Astrodynamics Specialist Conference*, No. AAS 68-084, American Astronautical Society, September 1968.